Proceedings of the 8th International Conference on MicroManufacturing
University of Victoria, Victoria, BC, Canada, March 25-28, 2013

High-speed Fabrication of Micro-channels using Line-based Laser Induced Plasma Micromachining (L-LIPMM)

ICOMM 2013
No. 66

Ishan Saxena[1], Rajiv Malhotra[2], Kornel Ehmann[3], and Jian Cao[4]

[1]Ishan Saxena; Dept. of Mechanical Engineering, Northwestern University, USA; ishan@u.northwestern.edu
[2]Rajiv Malhotra; Dept. of Mechanical Engineering, Northwestern University, USA; rajivmalhotra2013@u.northwestern.edu
[3]Kornel Ehmann; Dept. of Mechanical Engineering, Northwestern University, USA; k-ehmann@northwestern.edu
[4]Jian Cao; Dept. of Mechanical Engineering, Northwestern University, USA; jcao@northwestern.edu

ABSTRACT

Micro-texturing of surfaces has various applications that often involve texturing over large (macro-scale) areas with high precision and resolution. This demands scalability and speed of texturing while retaining feature sizes of the order of a few μm. Moreover, micro-channels are a versatile micro-feature that are often used in microfluidic devices and can be arrayed or joined to form patterns and free-form geometries. We present a technique to fabricate micro-channels on surfaces with high-speed and by using a multi-material process, namely Laser Induced Plasma Micromachining (LIPMM). The process has the potential to machine metals, ceramics, polymers and other transparent, brittle and hard-to-machine materials. The presented technique uses an optical system to modify the laser spot into the shape of a line, to fabricate micro-channels directly without scanning as in the case of a regular circular spot. The process schematics are shown, and micro-machining experiments on polished Aluminum are discussed. Moreover, it is shown that the depth and width of the channels may be varied by changing process parameters like the pulse energy, pulse frequency and number of exposures.

Key Words: Laser induced plasma micromachining, line plasma, micro-channels

INTRODUCTION

Micro-texturing over large surfaces has been used to impart surface properties such as enhanced hydrophobicity or hydrophilicity [1], retarded or accelerated bacteria and algae growth [2], increased light trapping for solar cells [3], friction reduction [4] and wear reduction in tools [5]. Micro-channels are the most commonly used surface micro-texturing geometry, and may be combined (translated, rotated or stacked) in form of arrays to produce more complex features over a large area. Presently, pulsed laser micromachining is the most popular tool for texturing micro-channels over surfaces, due to its high resolution, low achievable feature size, and geometrical accuracy [6, 7]. However, a setback with conventional laser-based micro-texturing is its inability to machine materials with high surface reflectivity, ablation coefficient and bulk transmittivity like glass, quartz and ceramics. Recently, the technique of Spot-based Laser Induced Plasma Micro-Machining (LIPMM) has been developed to address the limitations of conventional ultra-short pulse laser micro-machining [8, 9]. Its main advantages are adaptability to a wide range of materials and superior wall geometries. We propose a variation of the Spot-based LIPMM process by creating line plasma instead of spot plasma by using a suitable optical system, for machining micro-channels with greater speed and hence the designation Line-LIPMM or L-LIPMM.

PROCESS DESCRIPTION

A. UNDERLYING IDEA

The critical examination of the literature and of the present state-of-the-art suggests the need for a high-yield/throughput process that would be fast, and yet deliver the precision of laser micro-machining for the production of micro-channels on different materials, which would cater to a wide variety of applications. In its simplest form, like in the conventional LIPMM process, to form laser induced plasma, a laser beam is focused at a spot by means of an aberration-corrected diffraction limited compound lens, for which the theoretical spot size at the beam's waist is determined by the input beam diameter and the focal length of the focusing lens. Plasma, formed when the ionization potential of the dielectric is exceeded in the focal volume, expands and removes material from the substrate. It is evident that a beam can be brought to focus in different shapes and forms and manipulated by different optical lenses. Capitalizing on the advantages of LIPMM reflected in its better machinability and adaptability to different materials over conventional laser ablation, the proposed L-LIPMM process is expected to surpass a number of limitations such as repeatability, resolution, speed of texturing, and energy losses that are inherent in conventional Spot-based LIPMM, laser ablation-based texturing and other mask-based and interference-based texturing methods that.

B. OPTICAL SYSTEM

A basic optical system is developed to focus the beam into a line rather than a spot. This involves using a converging laser beam along with a cylindrical lens. A diffraction-limited converging lens focuses the collimated laser beam into a spot (Fig. 1(a)). When combined with a plano-convex cylindrical lens mounted coaxially with the converging lens, the beam achieves focus in the shape of a line, which can be used to

ablate micro-channels (Fig. 1(b)). Figure 2(a) and 2(b) show the corresponding spot and line plasma shapes respectively generated by a 9 mm ($1/e^2$) diameter Gaussian laser beam, when seen under a CCD camera. The length of the line is determined by both the curvature and placement of the cylindrical lens along the path of the beam. The focusing lens has a diffraction-limited performance and when used with a Gaussian beam brings the beam to focus with a circular spot size with a diameter given by the following relation, determined by solving the Fresnel integral for beam waist (minimum diameter condition):

$$D_s = \frac{4\lambda}{\pi}\frac{F}{D}$$

where, λ is the wavelength of the monochromatic laser beam, F is the effective focal length of the diffraction-limited converging lens, and D is the diameter of the input beam.

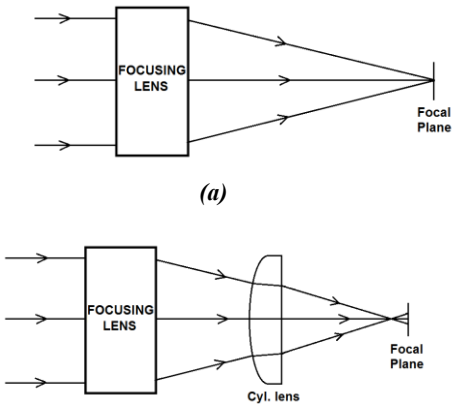

Fig.1: (a) Focal spot created with a converging lens, (b) Focal line created with a focusing lens and cylindrical lens.

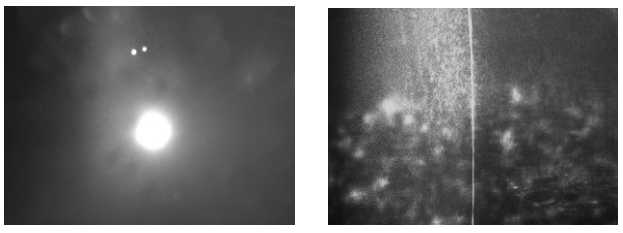

(a) ***(b)***

Fig.2: (a) Focal spot created with a converging lens, (b) Focal line created with a focusing lens and cylindrical lens.

C. OPTICAL SIMULATIONS

Ray tracing the marginal and principal rays through the optical system reveals that the focal shape is curved, as shown in Fig. 3(a). The beam output from the focusing lens and through the cylindrical lens can be seen from perpendicular cross-sections. From a first order analysis, the curvature of the focal line has been theoretically estimated at nearly one-third of the curvature of the plano-convex cylindrical lens. The position of the cylindrical lens determines the lateral spread (L_f) as well as the axial spread (d_f) of the focal line, see Fig. 3(b). Theoretical variation of the length and depth with the position of the plano-convex lens relative to the focusing triplet (d), is shown in Fig. 4 for a particular case in which the input beam diameter is assumed to be 6 mm ($1/e^2$), the focal length of the focusing lens to be 25 mm and that of the cylindrical lens to be 50 mm. It is evident that as the separation between the cylindrical lens and the triplet increases, the line length decreases, and the depth of focus increases. Hence, in order to obtain longer and less curved focal lines the lens must be placed at a shorter distance from the triplet (farther from the substrate). Although, the longer is the focal line, the lower is the intensity at the substrate.

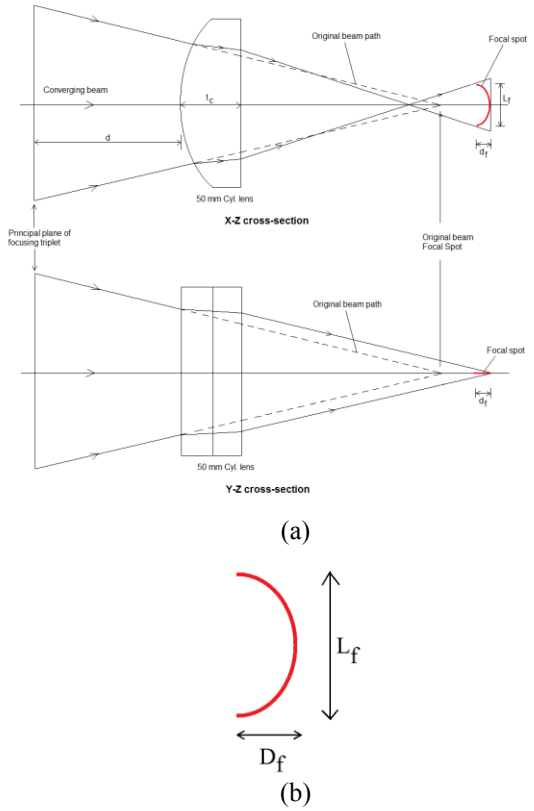

Fig. 3: Schematic representation of beam focal spot modification through the use of a cylindrical lens

The intensity distribution contour plots computed by near-field approximation to the Fresnel's integral, are shown for beam cross-sections at various distances along the Z-axis (along the direction of propagation) measured from the final surface of the cylindrical lens as seen in Fig. 5. It is evident that the beam achieves focus twice in the form of mutually perpendicular focal lines. Fig. 5(b) represents the near focal line and Fig. 5(g) represents the far focal line.

As shown by the preceding analysis, focal lines 1 mm in length and more can be produced by the optical system. Also, the

length of the line may be changed by translating the cylindrical lens axially closer to or farther away from the focusing lens. This translation also changes the focal line curvature and hence its axial spread.

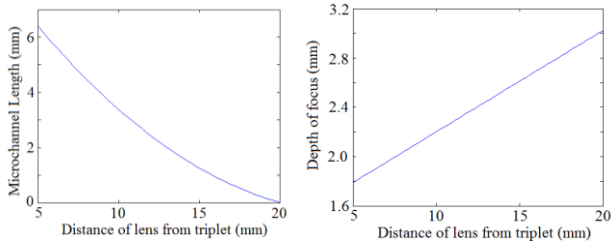

Fig. 4: (a) Length, and (b) Depth of the focal line, as a function of separation between the cylindrical lens and the focusing triplet.

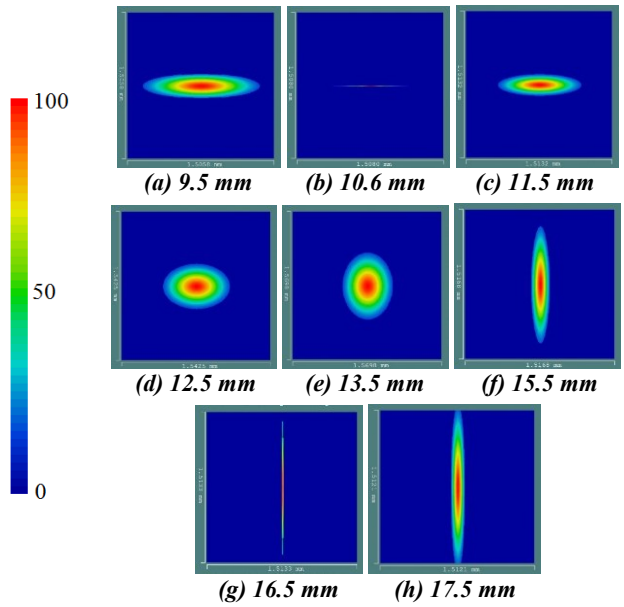

Fig. 5: Intensity distribution at different cross-sections along the axis of propagation. Note: focal spots approximately at (b) and (g)

EXPERIMENTS

A. EXPERIMENTAL SETUP

Preliminary experiments for L-LIPMM have been performed to establish proof of concept. This Section describes the laser system and the beam delivery setup for experimentation. The initial results demonstrate that a spot is expanded into a line using a cylindrical lens, whose characteristics depend on the beam parameters and optics. The controlling parameters are identified, and their effect on the machined micro-channels is presented.

The laser system used is a 532 nm wavelength Nd-YVO_4 pulsed laser with an 8 ps pulse duration operating at its second harmonic, manufactured by Lumera Lasers Inc. The beam profile is Gaussian, and the diameter from the laser exit is 0.6 mm ($1/e^2$). The beam is then expanded via two beam expanders, 3x and 5x sequentially, to increase the beam diameter to 9 mm. Collimation adjustment in the beam expanders is used to keep the beam collimated. Figure 6 shows the laboratory setup. The substrate is mounted on a 5-axis motion stage (Aerotech), which can translate in three directions and rotate along two axes. The translational resolution is 0.1 µm and rotational resolution is 0.001 degrees. A CCD camera is mounted for in-situ monitoring of the machining process from the point of view of the input beam. The laser can work at pulse frequencies ranging from 10 kHz to 500 kHz, and the beam power ranges from 0.03 W to 1.1 W, for the second harmonic (532 nm) beam.

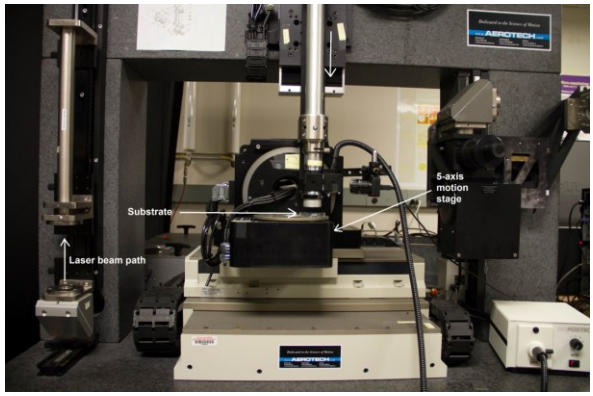

Fig. 6: Laser system, as shown with the beam delivery system and the 5-axis motion stage

The focusing triplet lens of effective focal length of 25 mm has a diffraction-limited performance, and when used with a Gaussian beam with a 9 mm ($1/e^2$) diameter brings the beam to focus with a theoretical spot size of approximately 7 µm in diameter. The plano-convex cylindrical lens of effective focal length 50 mm is made of UV fused silica, which has a refractive index of 1.46 at 532 nm, and a transmittivity greater than 97%/cm. Its center thickness is 5 mm, and the radius of curvature at the convex side is 22.93 mm.

B. ABLATED MICROFEATURES

Micro-channels 800-900 µm in length and 6-15 µm in width are machined by the line plasma generated by the cylindrical lens. The distance between the lens and the triplet is approximately 10 mm, and the exposure for each channel lasted for 20,000 pulses. The planar side of the cylindrical lens faces the substrate. The substrate used is polished aluminum, immersed in water which is the dielectric that facilitates plasma formation. Figure 7(a) shows a perspective view of three parallel micro-channels spaced 50 µm apart (center-to-center). A depth contour plot is shown in Fig. 7(b), and transverse depth profile cross-sections are shown in Fig. 7(c). The micro-channels are 6-8 µm wide and 26-30 µm deep. The substrate was ultrasonically cleaned prior to examination.

A. PROCESS PARAMETERS

A list of various beam parameters and other parameters used during the experiments is shown in Table 1. The controlling parameters are identified as depth control, pulse repetition rate, and beam intensity. A single exposure (or

exposure time) is defined as a sequence of laser pulses at the given repetition rate which are incident on the target workpiece, lasting about 3 seconds (30,000 to 1,500,000 pulses, depending on the pulse repetition frequency). The placement of the cylindrical lens has an effect on the length of the micro-channel. The far focal spot is used for micromachining of longer micro-channels.

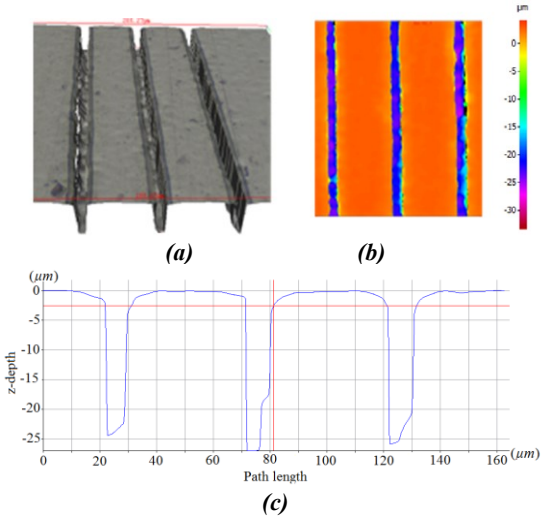

Fig. 7: (a) Perspective view, (b) depth contour plot, and (c) depth profile for micro-channels machined by L-LIPMM

Table 1: Experimental parameters

Parameter	Value
Beam Power	0.03 – 1.0 W
Pulse repetition frequency	10 – 500 kHz
Distance from focusing triplet to cylindrical lens	10 mm
Orientation of cylindrical lens	Planar side towards substrate
Substrate	Aluminum, Silicon
Dielectric	Kerosene, DI Water
Exposure time for each channel	3-4 seconds

As the beam intensity is not uniform along the length of the channel, the channel depth is expected to be the deepest in the middle portion. Assuming a Gaussian energy intensity distribution at the focal plane the $1/e^2$ length of the focal line is 203 μm. With 8 ps pulses firing at a 10 kHz repetition rates, the peak pulse power is therefore 1.875 MW. The peak energy density for the far focal spot is 1.4 x 10^{11}W/cm^2. In previous work, the energy density threshold required for creating plasma that can be used for micromachining with distilled water as the dielectric, has been determined to be 1.4 x 10^{11} W/cm^2 [9]. Hence, the energy densities of the focal lines at the near and far focal spots are equal to or greater than this critical energy threshold.

It was also observed that by using multiple exposures at different depths increased the depth of the micro-channels. The focal line was moved towards the substrate in increments of 2 μm between exposures, as shown schematically in Fig. 8. Each exposure lasts for 20,000 laser pulses, and the repetition rate was fixed at 20 kHz. The maximum depth obtained for each channel was measured, as well as the channel width at the maximum depth. Figure 9 shows the variation of channel depth and width with number of exposures.

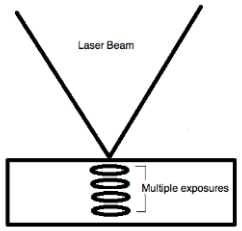

Fig. 8: Schematic of focal line variation process

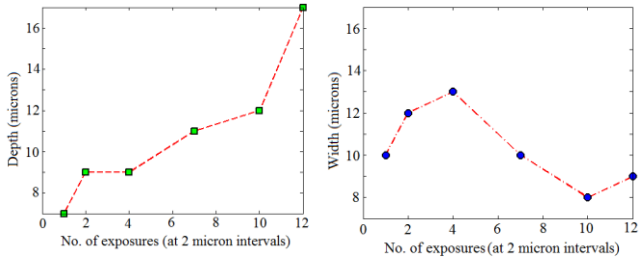

Fig. 9: Channel (a) depth and (b) width for different number of exposures

It is noticeable that with number of exposures, there is an increase in depth, although there is no particular trend observed in channel width. Figure 10 shows the deepest channel obtained, for 12 exposures.

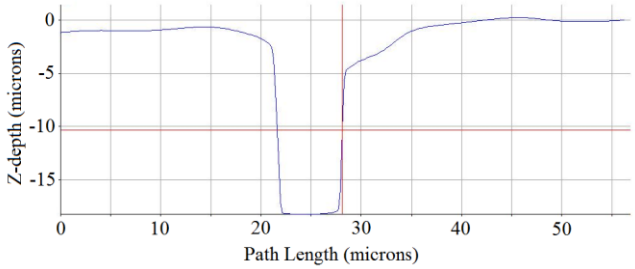

Fig. 10: Micro-channel after 12 exposures at 2 μm increments, deepest profile shown

Varying the pulse repetition rate increases the average power, but reduces the peak power (energy/pulse). Figure 11 graphically shows the variation of channel depth and width with pulse repetition rate. With an increase in repetition rate, the maximum channel depth first increases, then decreases. This is due to an increase and subsequent decrease in the pulse peak power. The maximum depth is obtained at 100 kHz, as seen in Fig. 12. The channel width stays approximately uniform, although there is a slight increasing trend at higher repetition rates.

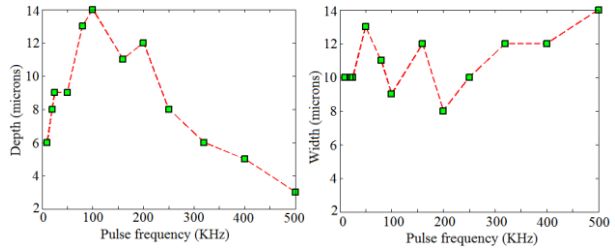

(a) *(b)*

Fig. 11: Effect of changing pulse frequency on (a) depth and (b) width of micro-channels

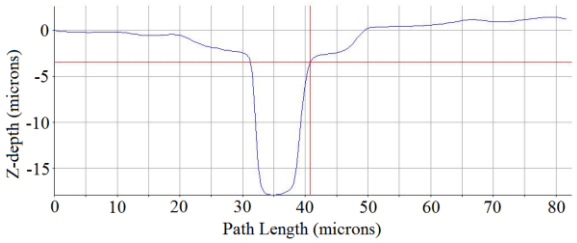

Fig. 12: Channel profile at maximum depth (100 kHz repetition rate)

The shape of the channel transitions from "V" to "U" at the mid-range of repetition rates, and then back to "V" at high repetition rates. In other words, channel walls change from tapered to near-vertical. Typical "V" and "U" shapes are shown in Fig. 13.

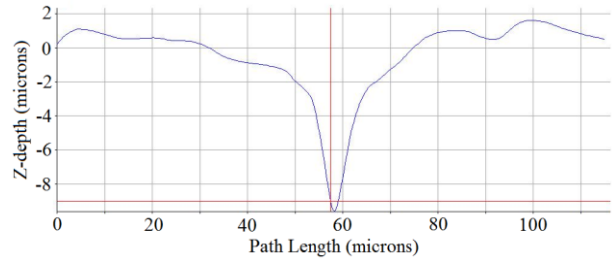

(a) Profile at 20 kHz repetition rate

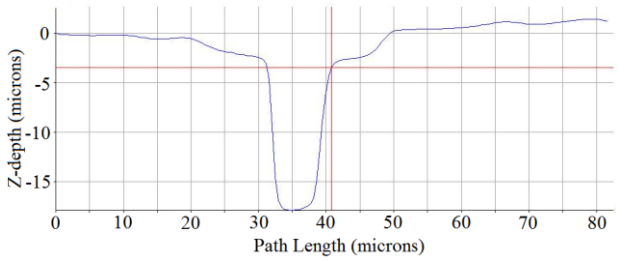

(b) Profile at 100 kHz repetition rate

Fig. 13: Channel profiles with tapered and near-vertical walls ("V" and "U" shapes)

The effect of varying the average beam power was also observed on channel depths and widths. While varying the average power, the pulse repetition rate is kept constant, thereby increasing the energy/pulse. Figure 14 shows the variation of channel depth and width for different frequencies at different beam average powers.

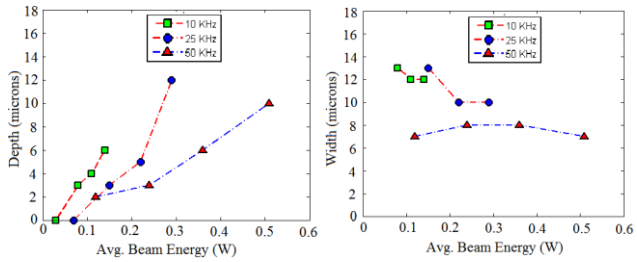

(a) *(b)*

Fig. 14: Effect of power variation on channel (a) depth and (b) width

Another noticeable effect of changing power is on the length of the channel. At a repetition rate of 50 kHz, the lengths of channels were observed for different beam intensities. Figure 15 shows an optical surface image of micro-channels of different lengths. At low frequencies and low power, the channel is not formed at all. Moreover, the width does not show any particular trend with change in average power.

As seen in Fig. 15, the formation of heat affected zones on Aluminum becomes more significant as the average beam intensity is increased. Also, the maximum heat affected zone is in the center of the channel, decreasing towards the ends.

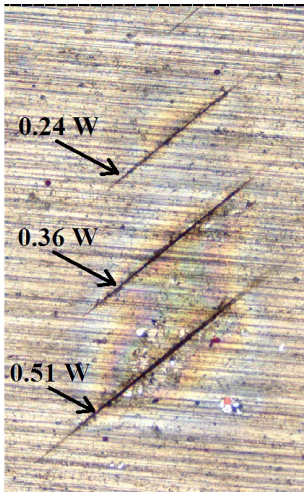

Fig. 15: Effect of changing power on the length of micro-channels, the power increases from top to bottom

The heat affected zones correspond with the intensity distribution along the length of the focal spot. As evident from the experimental results, the micro-channels are non-uniform throughout their length. The depth variation ranges from a few microns to about 10 microns.

C. TEXTURING OVER LARGE AREAS

Micro-channels were machined on an area of 6 mm x 6 mm on polished aluminum, by replicating a single micro-channel made by the line plasma method, over the entire area in the form of an array, as shown in Fig. 16 (perspective view). The channels were ablated at a 20 kHz pulse repetition rate and 0.3

W power, since this combination resulted in the most uniform geometry throughout the channel. The dielectric used for plasma creation was Kerosene. The length of each channel is 900 µm, while the lateral spacing between channels is 100 µm.

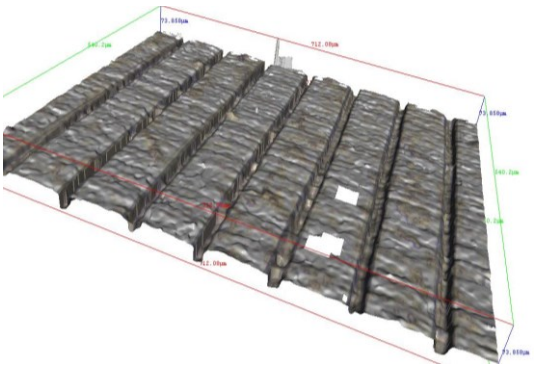

Fig. 16: Micro-channel array on Aluminum, 100 µm lateral spacing

The time required for machining each channel of about 1 mm length is 2 seconds. Using conventional focal spot ablation or spot plasma ablation by translating the spot at a speed of 5-10 µm/s (in order to achieve a similar geometry and depth), the time required to machine this would be between 100 – 200 seconds. Therefore, it is noticeable that there is a significant time reduction, of the order of 95-98%.

CONCLUSIONS

A high-speed process for fabrication of micro-channels and micro-channel arrays is presented. The underlying process for fabrication - LIPMM - has multi-material capability and can, therefore, be used to texture over a variety of substrates including metals, polymers, ceramics, optically transmissive and hard-to-machine materials. By L-LIPMM, the productivity of LIPMM has been enhanced by a factor of ≈20, by using an optical system to modify the beam focal spot shape and size. The beam parameters have a significant effect on the micro-channel depth and width. With multiple exposures, deeper channels may be obtained, without significant increase in width, hence increasing the aspect-ratio. Also, the highest depth of micro-channels is obtained at 100 kHz pulse frequency, and the channel cross-section profile changes from "V" to "U" shaped, with change in frequency. With an increase in average beam power, micro-channels are longer, and a more pronounced heat affected zone is also observed. The process may be used for large area surface texturing, with a significant increase in productivity.

REFERENCES

[1] J. Bico et al., "Wetting of textured surfaces," *Colloids and Surfaces A: Physicochemical and Engineering Aspects,* 2002; vol. 206 no. 1–3: 41-46.

[2] R. Bos et al., "Retention of bacteria on a substratum surface with micro-patterned hydrophobicity," *FEMS Microbiology Letters,* 2000; vol. 189 no. 2: 311-315.

[3] D. S. Hobbs et al., "Update on the development of high performance anti-reflecting surface relief micro-structures," 2007; pp. 65450Y.

[4] M. Nakano et al., "Applying Micro-Texture to Cast Iron Surfaces to Reduce the Friction Coefficient Under Lubricated Conditions," *Tribology Letters,* 2007; vol. 28 no. 2: 131-137.

[5] M. Geiger et al., "Excimer Laser Micro Texturing of Cold Forging Tool Surfaces - Influence on Tool Life," *CIRP Annals - Manufacturing Technology,* 2002; vol. 51 no. 1: 231-234.

[6] X. Liu et al., "Laser ablation and micromachining with ultrashort laser pulses," *Quantum Electronics, IEEE Journal of,* 1997; vol. 33 no. 10: 1706-1716.

[7] LIA Handbook of Laser Materials Processing, John F. Ready et al., Magnolia Publishing Inc.: 2001, 120-128.

[8] K. Pallav et al., "Comparative Assessment of the Laser Induced Plasma Micro-Machining (LIP-MM) and the Micro-EDM Processes," *ASME Journal of Manufacturing Science and Engineering (To appear)*, 2011.

[9] K. Pallav et al., "Feasibility of Laser Induced Plasma Micro-Machining (LIP-MM)," P*recision Assembly Technologies and Systems*, 2010; S. Ratchev, Ed., pp. 73-80**.**